Inorg. Chem. **2006**, *45*, 1130−1139

Supramolecular Asymmetric Induction in Dinuclear Triple-Stranded Helicates[1]

Robert M. Yeh and Kenneth N. Raymond*

Department of Chemistry, University of California, Berkeley, California 94720-1460

Received September 13, 2005

Supramolecular chiral induction has been observed in five dinuclear triple-stranded helicates composed entirely of achiral components. Three different chiral cations were found to be very effective at inducing high levels of enantiomeric enrichment in racemic mixtures of the helicates. The mechanism of intermolecular chiral induction in one cation–helicate pair, **s-nic/**$K_6[Ga_2\mathbf{L}^1{}_3]$, has been elucidated through circular dichroism spectroscopy, X-ray crystallography, and one and two-dimensional NMR spectroscopy (**s-nic** = *N*-methyl-s-nicotinium, $H_4\mathbf{L}^1$ = 1,4-bis(2′,3′-dihydroxybenzamido)phenylene).

Introduction

Chirality exists on many hierarchical levels. For example, an artificial D enantiomer of an HIV protease was shown to exhibit reciprocal chiral substrate specificity because the folded form of the synthetic D- and natural L-enzymes are mirror images of one another in all aspects of primary, secondary, and tertiary structure, including the substrate recognition site.[2] In other words, primary elements of chirality, such as the quaternary carbon centers in the individual amino acids, determine the tertiary structure of the enzyme active site, which ultimately controls the chirality of the recognized substrate.

Likewise, chirality in synthetic supramolecular complexes can be classified into several hierarchical levels. At the primary level, chirality can originate from chiral auxiliaries such as quaternary carbon stereocenters. Chirality on the secondary level can take the form of the handedness (R/S) of a helical structure or the twist direction (Δ/Λ) of a propeller structure. In a supramolecular ensemble, chirality on the secondary level disappears upon disassembly of the constituent components. In the absence of a primary source of absolute chirality, chirality on the secondary level manifests itself as a racemic mixture. Chirality on the tertiary level, such as asymmetric packing of helical coils in a liquid crystal, is governed by chirality on the secondary level.

We have previously demonstrated that the incorporation of carbon stereocenters at the extremities of a bis-bidentate catecholate ligand leads to the exclusive formation of one enantiomer of a dinuclear triple-stranded helicate.[3,4] There are many other examples in which a covalently integrated chiral auxiliary on the primary level determines the chirality of the supramolecular assembly on the secondary level.[5−21]

* To whom correspondence should be addressed. E-mail: raymond@socrates.berkeley.edu.

(1) Paper number 31 in the series Coordination Number Incommensurate Cluster Formation. For the previous paper in the series, see: Tiedemann, B. E.; Raymond, K. N. *Angew. Chem., Int. Ed.* **2006**, *45*, 83−86.

(2) Milton, R. C. D.; Milton, S. C. F.; Kent, S. B. H. *Science* **1992**, *256*, 1445−1448.
(3) Meyer, M.; Kersting, B.; Powers, R. E.; Raymond, K. N. *Inorg. Chem.* **1997**, *36*, 5179−5191.
(4) Kersting, B.; Meyer, M.; Powers, R. E.; Raymond, K. N. *J. Am. Chem. Soc.* **1996**, *118*, 7221−7222.
(5) Zarges, W.; Hall, J.; Lehn, J.-M. *Helv. Chim. Acta* **1991**, *74*, 1843−1852.
(6) Prins, L. J.; Huskens, J.; de Jong, F.; Timmerman, P.; Reinhoudt, D. N. *Nature* **1999**, *398*, 498−502.
(7) Prins, L. J.; Hulst, R.; Timmerman, P.; Reinhoudt, D. N. *Chem.−Eur. J.* **2002**, *8*, 2288−2301.
(8) Prins, L. J.; De Jong, F.; Timmerman, P.; Reinhoudt, D. N. *Nature* **2000**, *408*, 181−184.
(9) Cerero, S. D.; Bohme, M.; Nieger, M.; Vogtle, F. *Liebigs Annal./Recl.* **1997**, 1221−1225.
(10) Mamula, O.; von Zelewsky, A.; Bark, T.; Bernardinelli, G. *Angew. Chem., Int. Ed. Engl.* **1999**, *38*, 2945−2948.
(11) Ghizdavu, L.; Brunhilde, K.; von Zelewsky, A.; Stoeckli-Evans, H. *Eur. J. Inorg. Chem.* **1999**, 1271−1279.
(12) Knof, U.; von Zelewsky, A. *Angew. Chem., Int. Ed. Engl.* **1999**, *38*, 303−322.
(13) Baum, G.; Constable, E. C.; Fenske, D.; Housecroft, C. E.; Kulke, T. *Chem.−Eur. J.* **1999**, *5*, 1862−1873.
(14) Rivera, J. M.; Martin, T.; Rebek, J. *Science* **1998**, *279*, 1021−1023.
(15) Rivera, J. M.; Martin, T.; Rebek, J. *J. Am. Chem. Soc.* **2001**, *123*, 5213−5220.
(16) Amaya, T.; Rebek, J. *J. Am. Chem. Soc.* **2004**, *126*, 6216−6217.
(17) Stang, P. J.; Olenyuk, B. *Angew. Chem., Int. Ed. Engl.* **1996**, *35*, 732−736.
(18) Enemark, E. J.; Stack, T. D. P. *Angew. Chem., Int. Ed. Engl.* **1995**, *34*, 996−998.
(19) Masood, M. A.; Enemark, E. J.; Stack, T. D. P. *Angew. Chem., Int. Ed.* **1998**, *37*, 928−932.
(20) Woods, C. R.; Benaglia, M.; Siegel, S. J.; Cozzi, F. *Angew. Chem., Int. Ed. Engl.* **1996**, *35*, 1830−1833.

10.1021/ic0515711 CCC: $33.50
Published on Web 01/04/2006

In contrast to intramolecular chiral induction, supramolecular asymmetric induction relies on noncovalent interactions, such as van der Waals, π-stacking, and cation$-\pi$ contacts, to communicate chirality from one molecule to another. The most obvious manifestation of intermolecular asymmetric interaction is spontaneous resolution. For example, in the famous Pasteur resolution the spontaneous separation of racemic tartaric acid into enantiomerically pure D and L isomers is the result of favorable interactions between like isomers of tartaric acid.[22] In the realm of self-assembled structures, Lehn and co-workers described the spontaneous resolution of a racemic mixture of metallo-helicates into two enantiomers upon crystallization.[23] In other examples of intermolecular asymmetric induction, enantiomerically pure small molecules either induce enantiomeric enrichment in the racemic mixture of supermolecules in a dynamic equilibrium or resolve the mixture outright by selective precipitation or crystallization of one enantiomer. There are a number of reports in which the secondary and tertiary levels of chirality in a supramolecular system, composed entirely of achiral components, are controlled by noncovalent contacts with independent chiral molecules.[23−31] Chiral induction via asymmetric ion pairing has been recently reviewed.[32,33]

In this paper, we explore the roles of van der Waals contact and cation$-\pi$ interaction in communicating chirality to metallo-helicates self-assembled from achiral ligands. We report strong intermolecular asymmetric induction in five dinuclear triple-stranded helicates and focus on the mechanism of chirality information transfer via noncovalent contacts in one cation/helicate system.

Dinuclear Triple-Stranded Helicates. We have previously reported many anionic metal−ligand coordination assemblies based on bis-bidentate catecholate ligands.[34−36] The two primary architectures are the dinuclear triple-stranded helicates (D_3 symmetry) and the tetranuclear tetrahedra with idealized T_d symmetry (Figure 1). Both structures are inherently chiral because of the identical configuration at all the tris-bidentate-chelated metal centers within each coordination assembly. The two possible enantiomers of each structure, $\Delta\Delta$ or $\Lambda\Lambda$ helicates and $\Delta\Delta\Delta\Delta$ or $\Lambda\Lambda\Lambda\Lambda$ tetrahedra, exist as racemic mixtures in solution. In the case of the $K_{12}[Ga_4\mathbf{L}^N{}_6]$ tetrahedron ($H_4\mathbf{L}^N$ = 1,5-bis(2′,3′-dihydroxybenzamido)naphthalene), the racemates were resolved by coprecipitation of one enantiomer with *N*-methyl-s-nicotinium (**s-nic**), a methylated nicotine derivative.[37,38] On the basis of this initial result, we proceeded to investigate further the mechanism of chiral induction in catecholate containing coordination complexes.

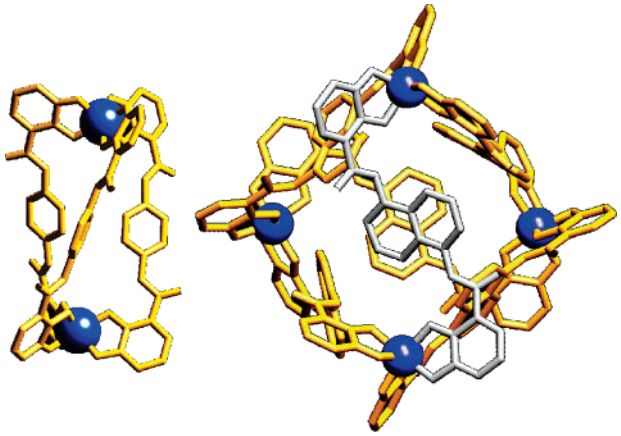

Figure 1. Anionic $M_2\mathbf{L}^1{}_3$ helicate (left) and $M_4\mathbf{L}^N{}_6$ ($H_4\mathbf{L}^N$ = 1,5-bis(2′,3′-dihydroxybenzamido)naphthalene) tetrahedron (right) have a similar anionic catecholate amide coordination environment around the metal ions. Their interactions with chiral cations are therefore expected to be similar.

This study focuses on dinuclear triple-stranded helicates rather than the more complicated tetranuclear tetrahedra for two reasons. First, the coordination environment near the metal centers is similar for the two architectures: both types of structures contain tris-catecholate chelated metal ions connected to aromatic backbones through amide linkages. Therefore, the mode of asymmetric interaction between the chiral cations and the anionic metal−ligand complexes is predicted to be similar for both types of assemblies. Indeed, in the crystal structure of the enantiomerically pure tetrahedron, all of the chiral countercations, although disordered and not fully resolved, are generally located around the anionic tris-catecholate metal vertexes rather than near the hydrophobic aromatic ligand backbone.[34] Second, coupling of two metal centers in the helicate, versus four in the tetrahedron, generates a lower energy barrier for racemization. As a result, at room temperature, the helicate exists as a mixture of racemizing enantiomers in dynamic equilibrium, whereas the tetrahedron exists as a static racemic population of enantiomers.[3,4] Therefore, for the helicates, the effectiveness of the chiral cation at communicating information regarding chirality can be correlated to the degree of enantiomeric enrichment induced by the chiral cation (Figure

(21) Zaworotko, M. J. *Angew. Chem., Int. Ed.* **1998**, *37*, 1211−1213.
(22) Natta, G.; Farina, M. *Stereochemistry*; Longman Group Limited: London, 1972.
(23) Kramer, R.; Lehn, J.-M.; De Cian, A.; Fischer, J. *Angew. Chem., Int. Ed. Engl.* **1993**, *32*, 703−706.
(24) Oda, R.; Huc, I.; Schmutz, M.; Candau, S. J.; MacKintosh, F. C. *Nature* **1999**, *399*, 566−569.
(25) Lehn, J.-M.; Hasenknopf, B. *Helv. Chim. Acta* **1996**, *79*, 1643−1650.
(26) Suarez, M.; Branda, N.; Lehn, J.-M.; Decian, A.; Fischer, J. *Helv. Chim. Acta* **1998**, *81*, 1−13.
(27) Jodry, J. J.; Lacour, J. *Chem.−Eur. J.* **2000**, *6*, 4297−4304.
(28) Lacour, J.; Jodry, J. J.; Monchaud, D. *Chem. Commun.* **2001**, 2302−2303.
(29) Borovkov, V. V.; Fujii, I.; Muranaka, A.; Hembury, G. A.; Tanaka, T.; Ceulemans, A.; Kobayashi, N.; Inoue, Y. *Angew. Chem., Int. Ed.* **2004**, *43*, 5481−5485.
(30) Borovkov, V. V.; Lintuluoto, J. M.; Inoue, Y. *J. Am. Chem. Soc.* **2001**, *123*, 2979−2989.
(31) Borovkov, V. V.; Lintuluoto, J. M.; Sugeta, H.; Fujiki, M.; Arakawa, R.; Inoue, Y. *J. Am. Chem. Soc.* **2002**, *124*, 2993−3006.
(32) Lacour, J.; Hebbe-Viton, V. *Chem. Soc. Rev.* **2003**, *32*, 373−382.
(33) Lacour, J.; Frantz, R. *Org. Biomol. Chem.* **2005**, *3*, 15−19.
(34) Caulder, D. L.; Brückner, C.; Powers, R. E.; Konig, S.; Parac, T. N.; Leary, J. A.; Raymond, K. N. *J. Am. Chem. Soc.* **2001**, *123*, 8923−8938.
(35) Caulder, D. L.; Raymond, K. N. *Angew. Chem., Int. Ed. Engl.* **1997**, *36*, 1440−1442.
(36) Caulder, D. L.; Raymond, K. N. *J. Chem. Soc., Dalton Trans.* **1999**, 1185−1200.
(37) Terpin, A. J.; Ziegler, M.; Johnson, D. W.; Raymond, K. N. *Angew. Chem., Int. Ed.* **2001**, *40*, 157−160.
(38) Ziegler, M.; Davis, A. V.; Johnson, D. W.; Raymond, K. N. *Angew. Chem., Int. Ed.* **2003**, *42*, 665−668.

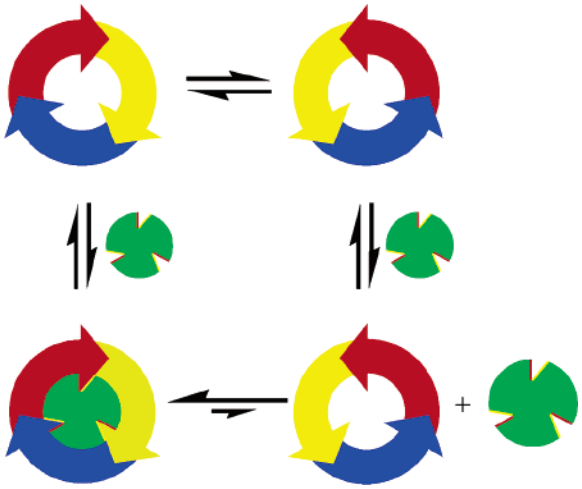

Figure 2. Schematic representation of racemates in dynamic equilibrium is shown as clockwise and counterclockwise rings. The source of chiral information, represented by the green insert, interacts more favorably with the clockwise ring, driving the equilibrium toward the clockwise enantiomer.

Scheme 1

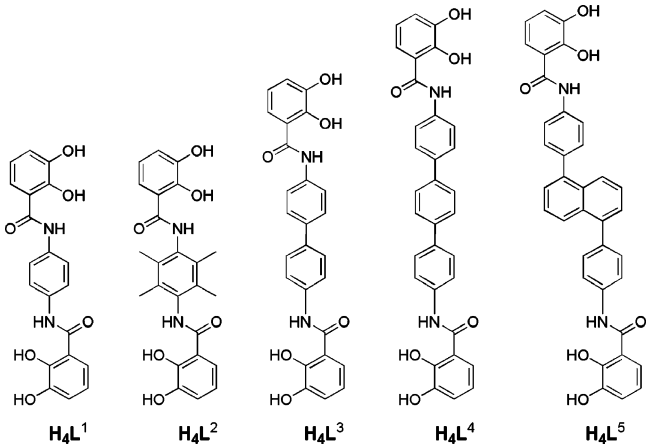

2). On the contrary, the two racemates of the tetranuclear tetrahedron are separated by coprecipitation with the chiral cation, and the resolved tetrahedra retain their chiral configuration even after prolonged heating and partial ligand exchange in the absence of the chiral cation.[37,38]

Five dinuclear triple-stranded helicates have been investigated for the effect of structural differences on chiral induction (Scheme 1).[3,4,35,39] The series of phenylene $[Ga_2\mathbf{L}^1{}_3]$,$^{6-}$ biphenylene $[Ga_2\mathbf{L}^3{}_3]$,$^{6-}$ and terphenylene $[Ga_2\mathbf{L}^4{}_3]^{6-}$ helicates have increased distance and rotational freedom between the two metal centers. The tetramethylphenylene $[Ga_2\mathbf{L}^2{}_3]^{6-}$ helicate adds steric bulk to the ligand backbone, which interferes with the chiral induction mechanism. The 1,5-phenylene-substituted naphthalene $[Ga_2\mathbf{L}^5{}_3]^{6-}$ helicate is reported here for the first time and contains staggered catecholate chelate vectors as opposed to the aligned chelate vectors of the other helicates (see Supporting Information for ^{1}H NMR and ESI-MS data of the $[Ga_4\mathbf{L}^5]^{6-}$ helicate and ref 33 for a description of chelate vectors).

Chiral Cations. Three chiral cations, *N*-methyl-s-nicotinium (**s-nic**), *N*-methyl cinchoninium (**cinc**), and *N*-methyl quininium (**quin**) were found to induce a chirality preference in the anionic helicates (Scheme 2). To ensure unambiguous transmission of chirality information, the cations must interact with each helicate in a stereospecific configuration and on a well-defined location of the helicate. The three cations share important structural motifs.

Scheme 2

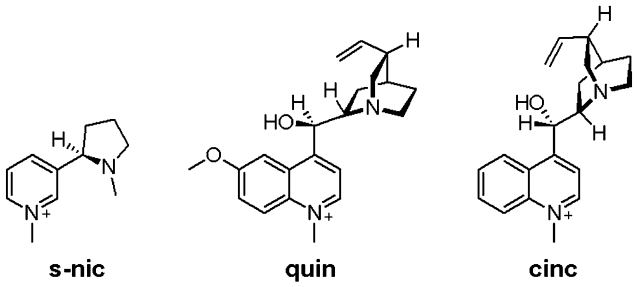

For all three chiral cations, methylation of the aromatic heterocycle (pyridine in the case of **s-nic** and quinoline in the cases of **cinc** and **quin**) yields large, flat cationic π acids that can bind to π-basic catecholate rings through cation$-\pi$ contact. In fact, an isomer of **s-nic** that has been methylated on the pyrrolidyl instead of pyridyl nitrogen does not induce a chiral preference in the helicate. This isomer of **s-nic** lacks a flat π-acidic ring that can firmly anchor the stereocenter onto the catecholate ring and highlights the critical importance of a strong $\pi-$cation interaction between the flat pyridinium cation of **s-nic** and the aromatic catecholate ring on the helicate.

Another feature common to all three chiral cations is the close proximity of a bulky group attached through a carbon stereocenter to the meta or para positions of the methylated heterocyclic ring. The appended large group serves to amplify the chiral information of the carbon stereocenter by projecting the steric bulk into an octant of space determined by the adjacent stereogenic carbon atom. Finally, note that the key structural difference between **cinc** and **quin** is the opposite configuration of the carbon stereocenter adjacent to the quinolinium ring.

Results and Discussion

UV−Vis Spectroscopy. The pale yellow solution of the helicate $K_6[Ga_2\mathbf{L}^1{}_3]$ and the colorless solution of **s-nic** become orange when mixed. The UV−Vis spectrum shows a small red shift of the helicate spectrum upon addition of **s-nic** iodide (Supporting Information S1). An absorption tail extending to above 450 nm gives rise to the orange color. This slight basochromic shift can be attributed to weak electronic coupling between the chiral cation and the catecholate ring of the helicate, which results in perturbation of the catecholate energy levels. A minor color change was also detected when **quin** or **cinc** were added to $K_6[Ga_2\mathbf{L}^1{}_3]$.

Circular Dichroism Spectroscopy. The degree of enantiomeric enrichment in the helicates was determined by circular dichroism spectroscopy. The three chiral cations exhibit negligible CD signals in the wavelength region and at the concentrations used in these studies. The CD spectra of the five helicates indicate some degree of chiral induction

(39) Scherer, M.; Caulder, D. L.; Johnson, D. W.; Raymond, K. N. *Angew. Chem., Int. Ed.* **1999**, *38*, 1588−1592.

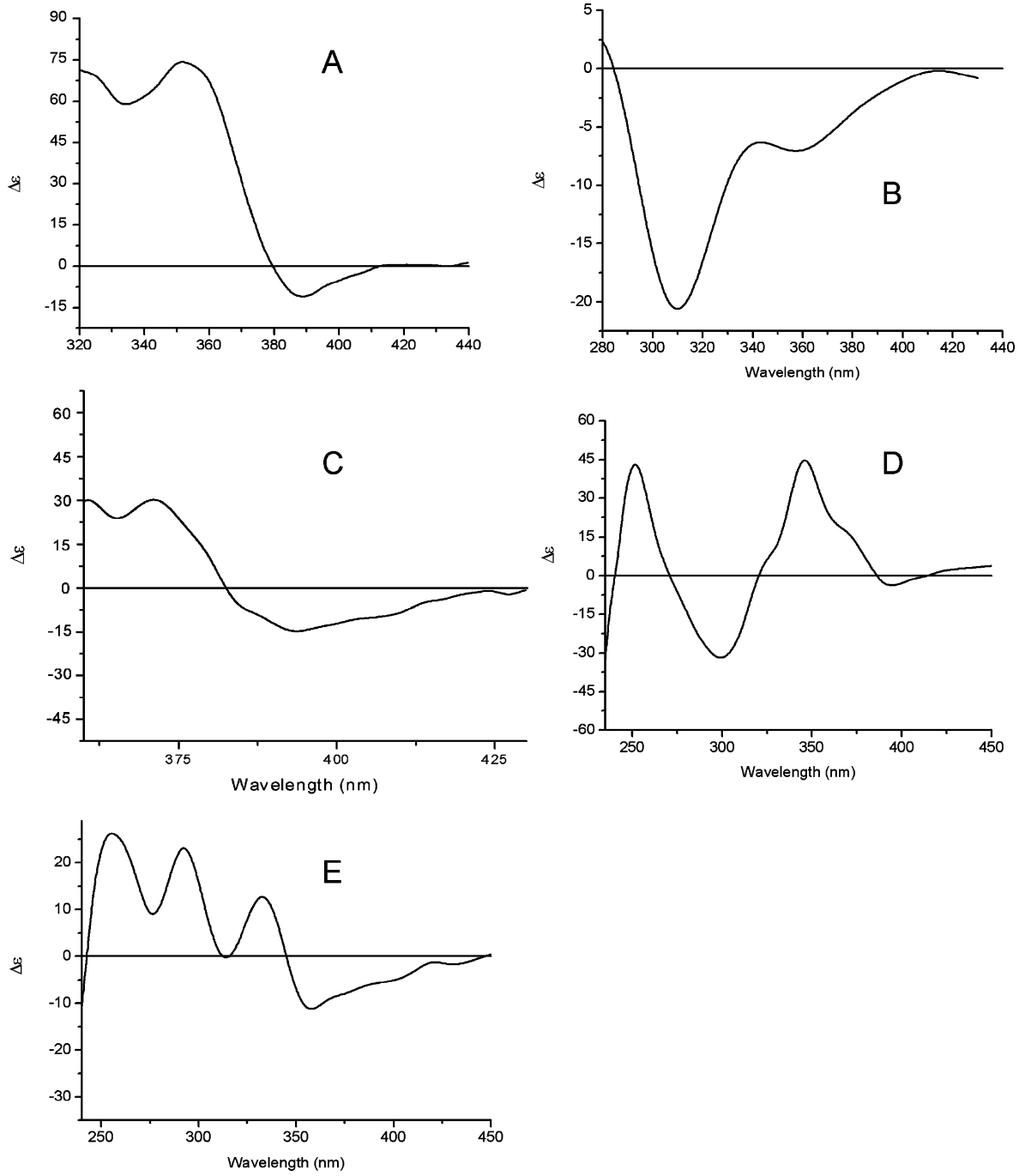

Figure 3. CD spectra of five helicates with **s-nic** iodide. The helicates from A to E are: $K_6[Ga_2\mathbf{L}^1{}_3]$, $K_6[Ga_2\mathbf{L}^2{}_3]$, $K_6[Ga_2\mathbf{L}^3{}_3]$, $K_6[Ga_2\mathbf{L}^4{}_3]$, and $K_6[Ga_2\mathbf{L}^5{}_3]$ (1 mM helicate in MeOH with 7 equiv of **s-nic** in a 0.1 mm round quartz cell, $\Delta\epsilon$ in M^{-1} cm^{-1}).

with **s-nic** in all cases, but the magnitude of enantiomeric enrichment varies (Figure 3). Notably, the tetramethylated derivative $[Ga_2\mathbf{L}^2{}_3]^{6-}$ exhibits a CD signal not only of significantly lower intensity but also of the opposite sign of the unmethylated $[Ga_2\mathbf{L}^1{}_3]^{6-}$ helicate. The phenyl $[Ga_2\mathbf{L}^1{}_3]^{6-}$, biphenyl $[Ga_2\mathbf{L}^3{}_3]^{6-}$, and terphenyl $[Ga_2\mathbf{L}^4{}_3]^{6-}$ helicates all exhibit significant degrees of induced chirality. The phenylene extended naphthalene helicate $[Ga_2\mathbf{L}^5{}_3]^{6-}$ has the most Cotton bands in the CD spectrum, consistent with it having the highest number of chromophores in its structure.

The CD bands for all the helicates are broad and complex; assignment of the bands to specific dipole−dipole interactions was not accomplished. Nevertheless, the lowest-energy Cotton band, between 350 and 380 nm, is observed in all helicates and is therefore attributed to the tris-catecholate moieties common to all the helicates. This lowest-energy band is used as a standard for determining the chirality and magnitude of asymmetric induction in the other spectra. In all the helicates, the bridging aromatic moieties are approximated as independent chromophores such that their dipoles are not interacting with the catecholate end units. The higher-energy bands originate from the interaction of the chromophores within the bridging aromatic groups. The number of these higher-energy bands increases with the increased size and complexity of the ligand aromatic bridge.

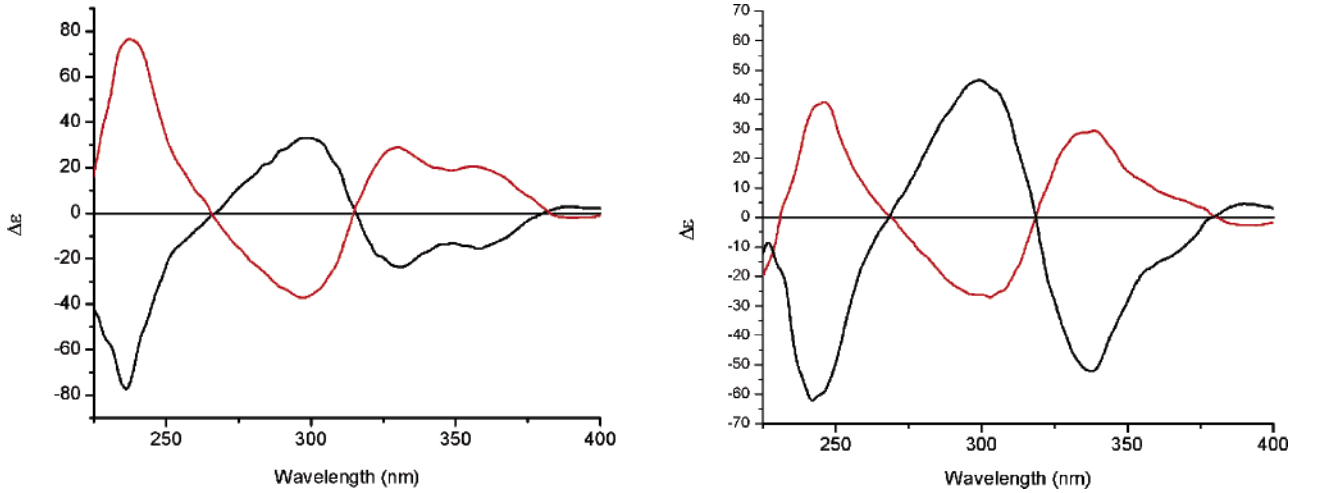

Figure 4. CD spectra of two different helicates, $K_6[Ga_2\mathbf{L}^3{}_3]$ (left) and $K_6[Ga_2\mathbf{L}^4{}_3]$ (right) with **cinc** (red line) and **quin** (black line) counterions added. (1 mM helicate in MeOH with 7 equiv of **cinc** or **quin** in a 0.1 mm round quartz cell, $\Delta\epsilon$ in M^{-1} cm^{-1}).

Two other chiral cations, **cinc** and **quin**, also induce enantiomeric enrichment in the helicates. As noted earlier, the key structural difference between **cinc** and **quin** is the opposite R and S configuration of the carbon stereocenter adjacent to the quinolinium ring. Consequently, the two ions induce opposite chirality in the helicates, as indicated by the inverted sign of all the Cotton bands in the spectra of a given helicate with the two different cations (Figure 4). Furthermore, the nearly perfect mirror images of the CD spectra further supports the assumption that the CD signals originate from the helicate and not the chiral cations, which have very different CD spectra (Supporting Information S2). Apparently the extra methoxy group on **cinc** has a negligible effect on the chirality induction of the cation.

All of the solution CD spectra were obtained in methanolic solutions at millimolar concentrations. No chiral induction was detected in water. Apparently the ionic interactions critical to chiral induction are attenuated in water compared to in the lower-dielectric solvent methanol. Numerous precedents in the literature, in particular several that involve chiral anions inducing chirality in cationic helical species, show the importance of strong asymmetric ion pairing in the chiral induction process.[40,41,42,43,44] An enantiomeric excess of nearly 100% has been achieved in some cases.

Solid-State Circular Dichroism Experiment. In addition to solution CD data, chirality of a bulk crystalline sample of $K(\mathbf{s\text{-}nic})_5[Ga_2\mathbf{L}^1{}_3]$ was confirmed by solid-state CD spectroscopy (Figure 5). The dried crystals were ground into a powder with potassium bromide and compressed into transparent disks (details of the solid-state CD measurements and $\Delta\epsilon$ calculation are described in the Experimental Section).

It is difficult to evaluate the absolute level of enantiomeric excess (ee) solely on the basis of the CD data. This has been an estimated by comparing the magnitude of the CD peak at approximately 350 nm between the dinuclear $[Ga_2\mathbf{L}^1{}_3]^{6-}$ helicate and the enantiomerically pure $[Ga_4\mathbf{L}^N{}_6]^{12-}$ tetranuclear tetrahedron. We assume that the peak at 350 nm results purely from the catecholate moieties, which are identical in both the helicate and the tetrahedron. Therefore

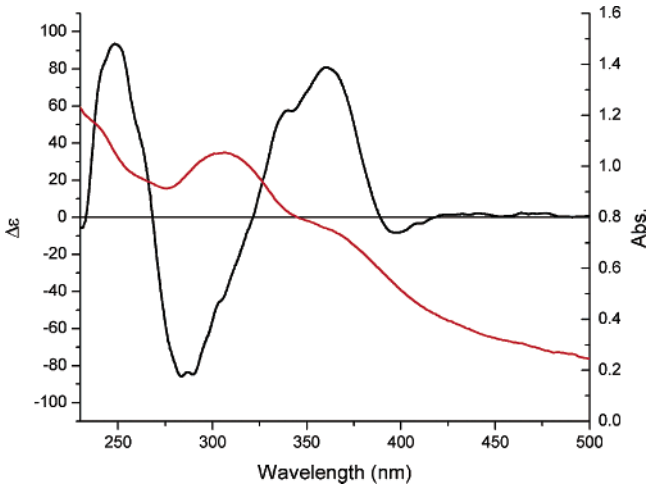

Figure 5. Solid-state CD spectrum (black line, averaged, smoothed) and UV−Vis spectrum (red line, smoothed) of $K(\mathbf{s\text{-}nic})_5[Ga_2\mathbf{L}^1{}_3]$.

a helicate with two tris-catecholate centers is expected to yield approximately half of the $\Delta\epsilon$ intensity as a tetrahedron which has four tris-catecholate centers. The solid-state spectrum of the helicate $K(\mathbf{s\text{-}nic})_5[Ga_2\mathbf{L}^1{}_3]$ shows a $\Delta\epsilon$ value of about 90 M^{-1} cm^{-1} at 350 nm in contrast to a $\Delta\epsilon$ value of 210 M^{-1} cm^{-1} for the enantiomerically pure $[Ga_4\mathbf{L}^N{}_6]^{12-}$ tetrahedron. This analysis would estimate the enantiomeric purity of the bulk crystalline sample of the helicate as 86%.

However, the actual ee in the bulk crystalline sample is likely to be greater than 86% since as the crystallization process draws the ΛΛ enantiomer out of solution from the dynamic equilibrium, the remaining ΔΔ helicates racemize to the ΛΛ configuration, and an ee value of 100% for the solid crystalline sample should eventually be observed. In our experiment, the bulk crystalline sample used for solid state CD analysis was invariably contaminated by a small but undetermined amount of amorphous material. This amorphous material is presumably a racemic mixture of helicates. Although the racemic helicates yield a UV absorption signal, which was used to determine the helicate concentration in the solid-state based on the extinction coefficient measured, they lower the overall magnitude of

Scheme 3

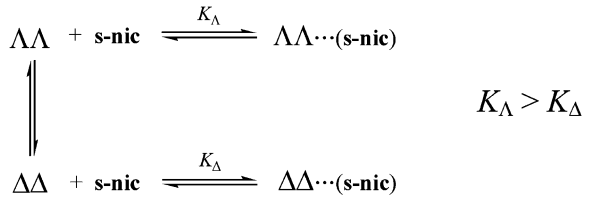

the CD signal. For the purpose of the equilibrium analysis described below, we assume that the solid sample has 100% ee.

Equilibrium Analysis of Chiral Induction. The maximum achievable $\Delta\epsilon$ in solution for the [$Ga_2\mathbf{L}^1_3$] helicate with any amount of **s-nic** is about 67 M^{-1} cm^{-1} at 350 nm, a value that is approximately 25% lower than the ee observed in the crystalline solid sample (90 L M^{-1} cm^{-1} at 350 nm). This observation can be rationalized by a dynamic equilibrium between the ΔΔ and ΛΛ helicates in solution. An equilibrium model between **s-nic** and the K_6[$Ga_2\mathbf{L}^1_3$] helicate was previously presented.[45] That model is summarized in this section and its relevance to the mechanism of chiral induction is discussed.

An equilibrium model between the ΔΔ and ΛΛ helicates is presented in Scheme 3. Potassium counterions are omitted from the model because the interaction of potassium with the two opposite enantiomers is degenerate. The more favorable binding of **s-nic** to the ΛΛ isomer means that K_Λ is greater than K_Δ, and therefore the equilibrium favors the ΛΛ helicate. Previous analysis showed that the binding affinity of **s-nic** for the ΛΛ helicate is about 6 times higher ($K_\Lambda/K_\Delta = 6 \pm 1.6$) than the affinity for the ΔΔ helicate. It follows that the energy difference $\Delta\Delta G$ between the ΛΛ and ΔΔ helicates in the asymmetric **s-nic** environment is about 1.1 (±0.2) kcal/mol. This free energy difference corresponds to a ΛΛ to ΔΔ isomer ratio of 85:15 at room temperature and therefore to an ee value of 70%. This value corresponds very well with the observed maximum ee value in solution of 75%, which is based on the assumption that the ee obtained in the solid state is 100%.

While there can be as many as six **s-nic** ions associated with each helicate, titration of **s-nic** ions into a solution of helicate shows that additional **s-nic** ions beyond the first one have a significantly diminished effect on chiral induction (Supporting Information Figure S3). In the following sections, we explore details of the intermolecular contact between the chiral cation and the helicate and determine the reason for the large induced ee with only one **s-nic** ion.

Mechanism of Supramolecular Asymmetric Induction. Crystal Structure of K(s-nic)$_5$[$Ga_2\mathbf{L}^1_3$]. A brief description of this crystal structure was presented in a previous communication;[45] we elaborate on this as an integral part of the discussion on the mechanism of chiral induction.

The diffusion of THF into a methanolic solution of K_6-[$Ga_2\mathbf{L}^1_3$] in the presence of six equivalents of **s-nic** iodide resulted in the crystallization of the ΛΛ isomer as K(**s-nic**)$_5$-[$Ga_2\mathbf{L}^1_3$]. The structure is chiral, and in space group $P2_1$. The refined structure has a Flack parameter value of 0.06 indicating a high level of confidence in its absolute chirality. The enantiomeric purity of the bulk crystalline sample was confirmed by solid-state CD spectroscopy as described earlier, and therefore this is not a case of spontaneous resolution. There are two helicates and 10 **s-nic** ions per unit cell. Despite the presence of more than six equivalents of **s-nic** iodide in the crystal growing medium, the crystal structure reveals five cocrystallized **s-nic** ions and one potassium ion per helicate (Figure 6). Fortuitously, as a result of having only five instead of six **s-nic** cations accompanying each helicate, there is no 3-fold crystallographic symmetry relating the **s-nic** ions. Therefore each **s-nic** ion was independently resolved without disorder or partial occupancy ambiguity. This is particularly useful for determining the exact intermolecular contacts between **s-nic** and the helicate that result in chiral induction.

Several different views of the helicate interacting with **s-nic** are shown in Figure 6. Each catecholate ring of the helicate is sandwiched between a pyridinium ring of a **s-nic** ion on one side and a pyrrolidine moiety from an adjacent **s-nic** ion. Each pyridyl nitrogen of **s-nic** is within 3.75 Å of the centroid of the nearest catecholate ring, and the pyridinium ring is parallel to the catecholate ring with an interplanar distance of 3.75 Å. This conformation allows strong cation−π interactions between the electron-poor pyridinium ring of **s-nic** (π acceptor) and the electron-rich catecholate ring (π donor). Each pyrrolidine unit of **s-nic** is angled away from the metal center, with the methylated tertiary nitrogen tilted away from the middle bridging phenylene of the helicate in a twist direction determined by the carbon stereocenter. There is a tight van der Waals contact between the protons of the pyrrolidine ring and the catecholate. The approximate 109° angle between the pyridinium and the pyrrolidine moieties allows for a good fit into the void defined by two adjacent catecholate rings which are spaced 120° apart.

In essence, the **s-nic** ion acts as a chiral wedge that sits in the cleft between the catecholate planes. As soon as one **s-nic** ion is inserted between two catecholates, the chirality of that metal center is fully determined. And since mechanical coupling between the metal centers in the helicate is strong, once chirality of one metal center is determined, the chirality of the entire helicate is set.[2] In the titration experiment 45% ee was observed, with only one **s-nic** ion per helicate, 60% ee with two **s-nic** ions, and a nearly saturated solution ee value of 70% with three **s-nic** ions (Supporting Information Figure S3). Significantly, the initial **s-nic**/helicate interaction is the most critical to the chiral induction process.

(40) Constable, E. C.; Frantz, R.; Housecroft, C. E.; Lacour, J.; Mahmood, A. *Inorg. Chem.* **2004**, *43*, 4817−4819.
(41) Frantz, R.; Pinto, A.; Constant, S.; Bernardinelli, G.; Lacour, J. *Angew. Chem., Int. Ed.* **2005**, *44*, 5060−5064.
(42) Jodry, J. J.; Frantz, R.; Lacour, J. *Inorg. Chem.* **2004**, *43*, 3329−3331.
(43) Martinez-Viviente, E.; Pregosin, P. S.; Vial, L.; Herse, C.; Lacour, J. *Chem.−Eur. J.* **2004**, *10*, 2912−2918.
(44) Monchaud, D.; Jodry, J. J.; Pomeranc, D.; Heitz, V.; Chambron, J. C.; Sauvage, J. P.; Lacour, J. *Angew. Chem., Int. Ed.* **2002**, *41*, 2317−2319.
(45) Yeh, R. M.; Ziegler, M.; Johnson, D. W.; Terpin, A. J.; Raymond, K. N. *Inorg. Chem.* **2001**, *40*, 2216−2217.

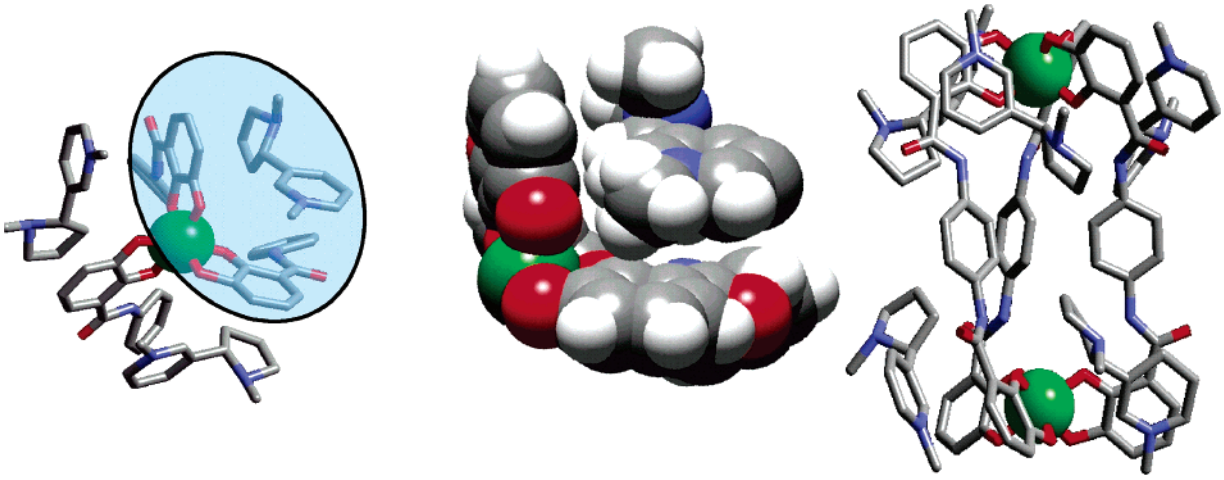

Figure 6. (right) Crystal structure of the helicate K(**s-nic**)$_5$[Ga$_2$**L**$^1_3$]. (left) Truncated view along the helicate 3-fold axis of the top tris-catecholate metal cap and three associated **s-nic** ions. (middle) Detailed space-filling (80% vdW) view of the interaction between two catecholate rings and one **s-nic** ion (gallium is the large green sphere).

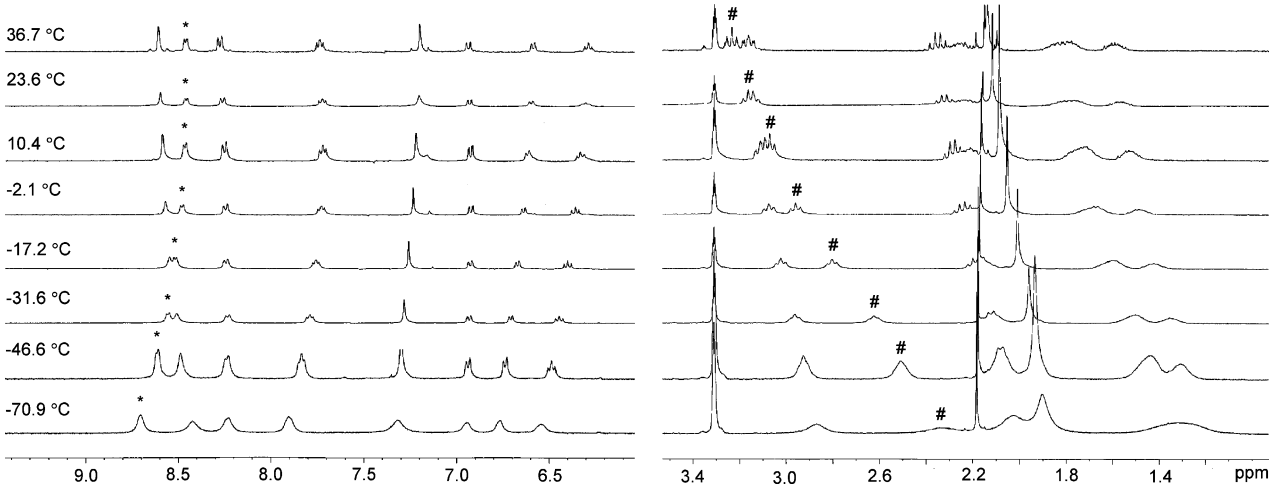

Figure 7. VT NMR spectra of K$_6$[Ga$_2$**L**$^1_3$] in the presence of 9 equiv of **s-nic** ion in MeOD-d$_4$. Concentration of **s-nic** is approximately 15 mM. The signals between 6 and 7 ppm belong to catecholate ring protons of the ligand **L**^{1}. The peak at approximately 7.3 ppm is assigned to the para-substituted phenylene backbone of **L**^{1}. * denotes a proton on the pyridinium moiety of **s-nic**; # denotes a pair of protons on the pyrrolidine unit of **s-nic**.

Chiral Induction in Mononuclear Tris-catecholate Complexes. No enantiomeric enrichment was observed when **s-nic** was added to mononuclear gallium tris-catecholate K$_3$Ga(L)$_3$ (L = 2,3-dihydroxy-4-(isopropylcarbamoyl)benzene). This result shows that catecholate interactions with **s-nic** pyridinium rings and pyrrolidine moieties alone are not sufficient to induce a chirality preference. Rather, a steric interaction of the **s-nic** pyrrolidine unit with the aromatic scaffold linking the tris-catecholate metal centers is essential for chiral induction.

VT and NOESY NMR Spectroscopy. The variable-temperature ^{1}H NMR spectra of K$_6$[Ga$_2$**L**$^1_3$] with **s-nic** in methanol-*d*$_4$ show strong and specific intermolecular interactions in solution. Large peak shifts corresponding to specific protons on the helicate [Ga$_2$**L**$^1_3$]$^{6-}$ and **s-nic** are observed in the VT ^{1}H NMR spectra. Figure 7 shows the dramatic movement of two peaks over the observed temperature range. As an example, the downfield peak (*) is assigned to a proton on the pyridinium ring while the upfield peak (#) belongs to a pair of protons on the pyrrolidine unit of **s-nic**. Other peaks belonging to the helicate, notably those of the protons on the catecholate rings, also show significant movement compared to that of the control spectra (Supporting Information Figure S4). The control spectra of pure helicate and pure **s-nic** show virtually no peak movement over the identical temperature range. Movement of the peaks in the K$_6$[Ga$_2$**L**$^1_3$]/**s-nic** mixture can be attributed to the temperature dependence of intermolecular interaction between the two species. At high temperature, the signals for **s-nic** (9 equiv/K$_6$[Ga$_2$**L**$^1_3$]) correspond to the coalesced signals of the ion paired and free **s-nic**. As the rate of exchange between the bound and free **s-nic** decreases with lower temperature, peak broadening is observed. Also, intermolecular contact is expected to become tighter with decreasing temperature, thus the magnitude of the peak shift is larger at lower temperature.

^{1}H NMR spectra obtained at −11 °C with different **s-nic** concentrations reveal sets of small helicate proton peaks adjacent to large helicate proton peaks. These peaks are especially noticeable at a **s-nic** to helicate ratio of 3.5:1 (Figure 8). There are a total of four aromatic proton signals belonging to the helicate. The large singlet at approximately 7.2 ppm is assigned to the protons on the phenylene backbone

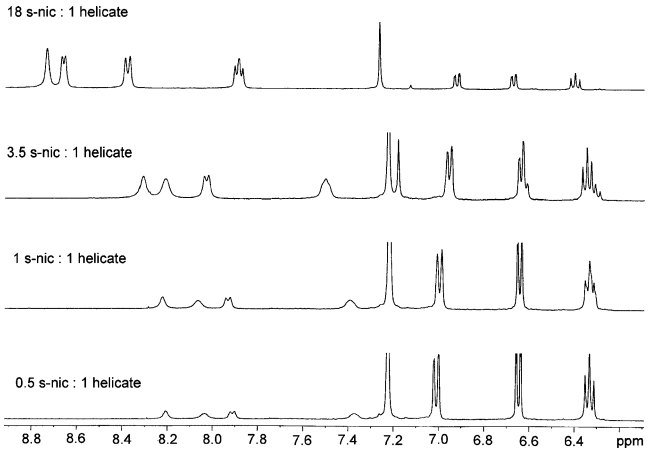

Figure 8. In the presence of 3.5 equiv of **s-nic** to 1 equiv of $K_6[Ga_2L^1{}_3]$ helicate, diastereotopic pairs of the ΔΔ-**s-nic** and ΛΛ-**s-nic** helicate ion pairs are easily distinguishable by ^{1}H NMR spectroscopy.

of the helicate. The set of two doublets and a triplet between 6.3 and 7.0 ppm are assigned to the catecholate units. The set of small helicate peaks adjacent to the large helicate proton peaks is attributed to the minor population of ΔΔ helicate present in the strongly asymmetric environment imposed by a high concentration of **s-nic** and is most visible at −11 °C because the rate of ion exchange slows down sufficiently to allow distinction between the two diastereotopic ion pairs on the NMR time scale. The temperature was chosen on the basis of the data from the VT NMR experiments described above, which showed maximum asymmetric induction and peak shift at −11 °C. Lower temperatures caused precipitation of ion paired complexes, while higher temperatures decreased the amount of peak shift because of weakened intermolecular contacts. The ratio between the ΛΛ and ΔΔ helicate isomers is 1:1 at zero molar **s-nic** and shifts in favor of the ΛΛ isomer as **s-nic** concentration increases. At a low concentration of **s-nic**, when nearly half of the helicates are present as the ΔΔ isomer, only one set of helicate signals is observed because the solution is not a sufficiently strong chiral shift environment to distinguish between the two enantiomers. The ratio of the integrated areas under the large versus the small sets of helicate peaks is about 1:3 at a **s-nic** to helicate ratio of 3.5:1. This ratio of enantiomers corresponds to an ee of 50%, which is about 20% lower than the value obtained from the CD experiments at the same **s-nic** to helicate ratio. The NMR integration data cannot be used as a reliable means of determining ee because there is partial coalescence of the NMR proton peaks caused by the dynamic equilibrium.

Two-dimensional NOESY experiments show cross-peaks between the proximate protons of helicate $K_6[Ga_2\mathbf{L}^1{}_3]$ and **s-nic**. The NOESY spectrum shown in Figure 9 was obtained at −11 °C to maximize peak intensity and sharpness. The Overhauser effect decreases rapidly with distance ($\propto d^{-6}$) and intermolecular NOE generally is not observed beyond a proton−proton distance of 4 Å. The spectrum shows strong cross-peaks that indicate not only tight ion-pair association at approximately 4 Å but also that **s-nic** interacts with the helicate in a similar conformation in solution and the solid

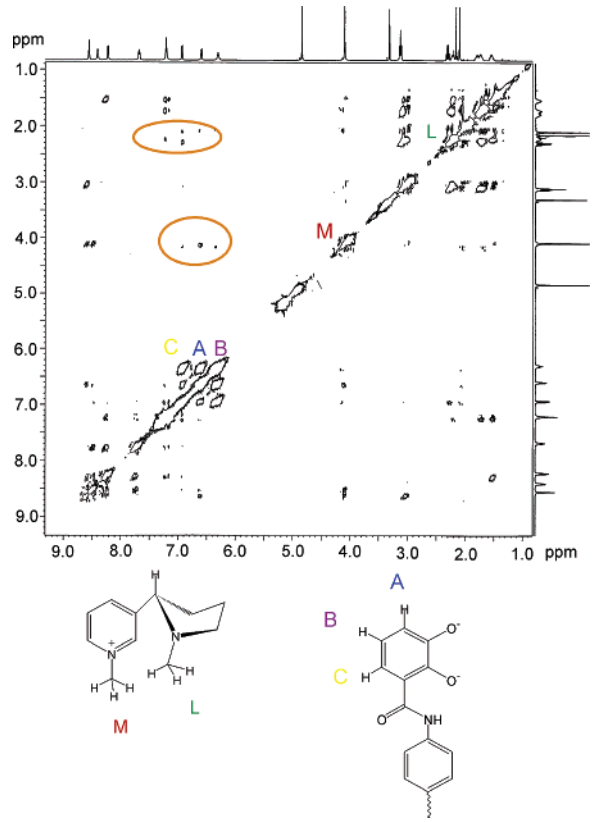

Figure 9. NOESY spectrum of $K_6[Ga_2\mathbf{L}^1{}_3]$ in MeOD-d_4 at 2 mmol and 9 equiv of **s-nic**. Interactions between the key protons are highlighted by color.

state. In Figure 9, the protons that give rise to the cross-peaks are labeled on both the catecholate unit and **s-nic** ion. The positions of these interactions indicate that **s-nic** binds to the catecholate moiety in the same configuration in solution as in the solid state, with the methyl groups on both the pyridine and pyrrolidine rings pointed away from the bridging body of the helicate.

Conclusion

We have shown that the point chirality of **s-nic** is communicated to the helicate $[Ga_2\mathbf{L}^1{}_3]^{6-}$ through cation−π and van der Waals contacts imposed by the plane-to-plane anchored π-acidic pyridinium and the bulky pyrrolidine groups. Because of the precise nature this interaction, minor variations in the structures of the chiral cation as well as the central scaffold of the helicate can have large effects on the level of intermolecular chiral induction. For example, methylation of nicotine on the pyrrolidyl instead of the pyridyl nitrogen completely eliminates chiral induction. In another example, whereas the additional methoxy group on **quin** (as opposed to **cinc**) has negligible effect on the ability of that cation to induce a chirality preference in the helicates, the addition of methyl groups to the phenylene backbone of $H_4\mathbf{L}^1$ (to form $H_4\mathbf{L}^2$) results in drastically diminished chiral induction. In the $[Ga_2\mathbf{L}^2{}_3]^{6-}$ helicate, the pyrrolidine moiety of **s-nic**, if positioned in the same configuration as in $K($**s-nic**$)_5[Ga_2\mathbf{L}^1{}_3]$, would be pushed into the ortho methyl groups on the ligand scaffold. This steric congestion may explain the weak chiral induction in $[Ga_2\mathbf{L}^2{}_3]^{6-}$ despite having the

catecholate regions in common with the other helicates. Furthermore, to avoid this steric congestion, the **s-nic** ion may be positioned "up-side down" with respect to the $[Ga_2\mathbf{L}^2_3]^{6-}$ helicate as compared to the other helicates. In this reversed configuration, **s-nic** would induce the Δ configuration rather than Λ configuration in the tris-catecholate moiety, resulting in an inverted CD spectrum (Figure 3).

These results suggest that pyridinium- and quinolinium-based chiral salts other than **s-nic**, **cinc**, and **quin** may also act as strong chiral-induction or resolving agents for tris-catecholate-based metal complexes. The strong ion pairing between chiral cations and the helicates, coupled with cooperativity between the metal centers, means that only one chiral ion per helicate is necessary for a significant level of intermolecular asymmetric induction. By inducing chirality via noncovalent forces rather than direct covalent linkage of a chiral component to the helicate structure, the chirality of the helicate can be reversed by replacing the chiral ion with one of opposite chirality.

Experimental Procedures

General Methods. The ligands 1,4-bis(2′,3′-dihydroxybenzamido)phenylene $H_4\mathbf{L}^1$, 1,4-bis(2′,3′-dihydroxybenzamido)-2,3,5,6-tetramethyl-phenylene $H_4\mathbf{L}^2$, 4,4′-bis(2′,3′-dihydroxybenzamido)-1,1′-biphenyl $H_4\mathbf{L}^3$, and 4,4''-bis(2′,3′-dihydroxybenzamido)-1,1′:4′,1″-terphenyl $H_4\mathbf{L}^4$ were synthesized according to literature procedures. [3,4,35] The enantiomerically pure (+)-cinchoninium iodide, (−)-quininium iodide, and *N*-methyl-s-nicotinium iodide salts were synthesized according to literature procedures. [46−48]

All NMR spectra were recorded using Bruker AM400 and DRX500 spectrometers rated at 400 and 500 MHz for ^{1}H and equipped with Bruker BT1000 and BT3000 variable-temperature controllers, respectively. The ^{1}H NMR peaks are reported as shifts (ppm) downfield from TMS and referenced to residual solvent protons. UV−vis spectra were recorded using a HP 8453 spectrometer. Solution and solid-state CD spectra were recorded with a JASCO 500C spectropolarimeter.

For the solid-state CD spectrum, a crystalline sample of K(**s-nic**)$_5[Ga_2\mathbf{L}^1_3]$ was ground to a fine powder with potassium bromide and compressed into several orange transparent disks (thickness = 0.80 mm for the sample shown). Between scans, the disks were rotated 90 ° in plane to eliminate the linear dichroism component by averaging the spectra. The UV−Vis absorbance of the sample pellet was measured to obtain a calculated effective concentration in the solid state. The effective concentration of the helicate in the sample disk shown is 0.042 mmol.

For the solution CD spectra, methanolic solutions of the pure helicates and chiral cations were freshly prepared and allowed to incubate for a minimum of 30 min before data acquisition. Samples of different stoichiometries and concentrations for the titration experiment were prepared from stock solutions and allowed to equilibrate for a minimum of 30 min. Circular quartz cells of 0.1, 1.0, and 10.0 mm path lengths were used to obtain the spectra depending on the sample concentration. The UV−Vis absorbance of each sample is recorded in the same quartz cells.

4-Bromo-(2′,3′-dimethoxybenzamido)benzene. A dry Schlenk flask (250 mL) was charged with 2,3-dimethoxybenzoic acid (10 g, 55 mmol). Thionyl chloride (50 mL) was added to the flask while the slurry was vigorously stirred. DMF was immediately added to the slurry dropwise (approximately 0.5 mL) until the solid completely dissolved. The reaction was stirred under an inert atmosphere for 1 h with a gas bubbler. The solution was evaporated in a 30 °C water bath to dryness under vacuum (<0.001 Torr) on a Schlenk line. Dry CH_2Cl_2 (50 mL) was transferred to the beige solid to dissolve the residue. After the solid had dissolved (with sonication), the solution was evaporated to dryness with slight heating and kept under vacuum at room temperature for 1 h. The acid chloride was used without further purification or characterization. A Schlenk flask was charged with 4-bromoaniline (9.5 g, 55 mmol), 2,3-dimethoxybenzoic acid chloride (55 mmol, as prepared above), NEt_3 (8.5 mL, 60 mmol), and degassed CH_2Cl_2 (400 mL, dried over alumina sieves). The solution was filtered after 12 h of stirring at room temperature. The filtrate was washed with 1 M NaOH (3 × 100 mL) and 1 M HCl (3 × 100 mL). After it was dried with sodium sulfate, the CH_2Cl_2 solution was evaporated to yield a crude product. The solid was dissolved in a small volume of ethanol at reflux and allowed to cool slowly to room temperature. An off-white crystalline product was isolated. A second crop of product was isolated from a reduced volume of the ethanol (15.4 g, 84%). FAB MS: *m*/*z* 336 (40) $[M]^+$. ^{1}H NMR (400 MHz, $CDCl_3$): δ 10.08 (s, 1H), 7.78 (dd, J = 8 Hz, J = 1.6 Hz, 1H), 7.60 (d, J = 9.2 Hz, 2H), 7.48 (d, J = 9.2 Hz, 2H), 7.22 (t, J = 8 Hz, 1H), 7.12 (dd, J = 8 Hz, J = 1.6 Hz, 1H), 3.94 (s, 3H), 4.00 (s, 3H). ^{13}C NMR (100 MHz, DMSO): δ 165.4, 152.9, 146.2, 138.8, 131.9, 131.6, 124.6, 121.9, 120.3, 115.5, 115.1, 110.4, 61.5, 59.3, 30.8. Calcd (anal.) for $C_{15}H_{14}BrNO_3$: C, 53.59 (53.87); H, 4.20 (4.53); N, 4.17 (4.05).

4-Pinacolatoboronic Ester-(2′,3′-dimethoxybenzamido)benzene. A DMSO solution (50 mL, dry) of 4-bromo-(2′,3′-dimethoxybenzamido)benzene (0.50 g, 1.5 mmol), bis-pinacoldiborane (0.42 g, 1.7 mmol, 1.1 equiv), and the catalyst $PdCl_2(dppf)_2$ (5 mol %, 61 mg, dppf = diphenylphosphinoferrocene) was kept under a nitrogen atmosphere. An excess (more than 1.5 equiv) of KOAc (0.45 g) was added at room temperature. The mixture was stirred for 16 h at 85 °C. The very dark solution was filtered, diluted with water (100 mL) and brine (100 mL), and extracted with benzene (2 × 200 mL). The combined benzene layer was washed with water (3 × 100 mL) and brine (2 × 100 mL) and dried over sodium sulfate. Flash silica column chromatography (eluted with 40:1 $CHCl_3$/EtOAc) yielded 0.34 g of a white product (60% yield). ^{1}H NMR (400 MHz, $CDCl_3$): δ 10.05 (s), 7.83 (d, J = 9.5 Hz, 2H), 7.78 (dd, J = 8.0 Hz, J = 1.6 Hz, 1H), 7.70 (d, J = 9.5 Hz, 2H), 7.20 (t, J = 8.0 Hz, 1H), 7.08 (dd, J = 8.0 Hz, J = 1.6 Hz, 1H), 3.99 (s, 3H), 3.91 (s, 3H), 1.34 (s, 12H). Calcd (anal.) for $C_{21}H_{26}BNO_3 \cdot 0.5(CHCl_3)$: C, 58.30 (58.42); H, 6.03 (6.39); N, 3.16 (3.17). Following this procedure, the addition of 1 equiv of dppf/mol of catalyst improved the yield to approximately 75%.

1,5-Diiodonaphthalene. In an adaptation of a literature procedure,[49] a solution of 1,5-diaminonaphthalene (6.0 g, 38 mmol) in glacial acetic acid (50 mL) was added dropwise to a vigorously stirred cold (0 °C) solution of sodium nitrite (6 g, large excess relative to 1,5-diaminonaphthalene) in concentrated sulfuric acid (50 mL). The slow addition was controlled to ensure that the solution remained below 5 °C. After the addition was completed, the solution was poured into a large (1000 mL) beaker filled with ice (100 g) and urea (1 g). The large beaker was placed inside a

(46) Piette, V.; Lindner, W.; Crommen, J. *J. Chromatogr., A* **2000**, *894*, 63−71.
(47) Ramuz, H. *Helv. Chim. Acta* **1975**, *58*, 2050−2060.
(48) Seeman, J. I.; Whidby, J. F. *J. Org. Chem.* **1976**, *41*, 3824−3826.
(49) Rodriguez, J. G.; Tejedor, J. L. *J. Org. Chem.* **2002**, *67*, 7631−7640.

large ice bath to ensure that the solution remained at 0 °C. The brown ice slush containing 1,5-bis-diazoniumnaphthalene was poured into another beaker filled with a solution of potassium iodide (300 g KI, 300 mL H_2O). The mixture was gradually warmed to room temperature and stirred for 3 h. The dark brown slurry was filtered through a large Buchner funnel. The solid residue was extracted with CH_2Cl_2 (5×). The combined organic fractions were dried with sodium sulfate. The product was crystallized from toluene at reflux as brown needles in three crops (7.8 g, 54%). FAB MS: *m*/*z* 380 (100) $[M]^+$. ^{1}H NMR (500 MHz, DMSO-d_6): δ 8.22 (d, 2H), 8.07 (d, 2H); 7.40 (t, 2H). Calcd (Anal.) for $C_{10}H_6I_2$: C, 31.61 (31.90); H, 1.59 (6.67); N 0.0 (0.0).

1,5-Bis(4′-(2″,3″-dimethoxybenzamido)phenyl)naphthalene (Me$_4$L^5). A Schlenk flask was charged with 1,5-diiodonaphthalene (1.1 g, 2.9 mmol), 4-(2′,3′-dimethoxybenzamido)benzyl pinacol boronic ester (2.3 g, 6.0 mmol), degassed DMF (150 mL), and water (2.5 mL). Under a N_2 atmosphere, $Pd(PPh_3)_4$ (300 mg, 5 mol %), anhydrous K_3PO_4 tribasic (3.0 g), and Na_2CO_3 (2.0 g) were added to the solution. The mixture was stirred for 12 h at 100 °C under N_2. The reaction was cooled to room temperature, and 700 ml of 50% brine was added to precipitate a large quantity of a white solid. The solid was isolated by filtration and washed with water to remove residual DMF and base. The aqueous layer was extracted with CH_2Cl_2 (3 × 100 mL). The solid isolated earlier by filtration was dissolved into the organic layer which was washed with brine (3×), dried over sodium sulfate, filtered through a plug of silica gel (3 cm), and evaporated to dryness. The solid was washed with hot acetone. Repeated crystallization from hot ethanol yielded an off-white powder as a pure product. In some attempts to make this compound, flash silica column chromatography was necessary for the removal of residual unreacted starting material if it was present in significant quantities as determined by TLC. Yield: 1.41 g, 76%. FAB-MS: *m*/*z* 638 [M+]. ^{1}H NMR (400 MHz, $CDCl_3$): δ 10.15 (s, 2H), 7.97 (d, 2H), 7.85 (d, 2H), 7.84 (t, 4H), 7.57 (d, 4H), 7.52−7.47 (m, 4H), 7.25 (t, 2H), 7.13 (d, 2H), 4.08 (s, 6H), 3.95 (s, 6H). ^{13}C NMR ($CDCl_3$): δ 163.1, 152.7, 147.3, 140.0, 137.6, 137.0, 132.1, 130.8, 127.0, 126.9, 125.7, 125.5, 124.9, 123.0, 120.1, 115.8. Calcd (anal.) for $C_{40}H_{34}N_2O_6$: C, 75.22 (74.73); H, 5.37 (5.36); N, 4.39 (4.28).

1,5-Bis(4′-(2″,3″-dihydroxybenzamido)phenyl)naphthalene (H$_4$L^5). BBr_3 (approximately 20 equiv) was added to a solution of the protected ligand in CH_2Cl_2. The yellow heterogeneous mixture was stirred for 72 h at room temperature. All volatile material was evaporated under vacuum, and methanol was added to the solid. The methanol was evaporated under vacuum, and the solid was suspended in water and heated to reflux for 24 h. The white solid was isolated by filtration and dried under vacuum. FAB-MS: *m*/*z* 582 [M+]. ^{1}H NMR (300 MHz, DMSO): δ 11.62 (s, 2H), 10.50 (s, 2H), 9.46 (s, 2H), 7.86 (d, 4H), 7.58−7.45 (m, 10H), 6.99 (d, 4H), 6.79 (t, 2H). Calcd (Anal.). for $C_{36}H_{26}N_2O_6 \cdot 0.5H_2O$: C, 73.09 (72.86); H, 4.60 (4.53); N, 4.74 (4.61).

K$_6$[Ga$_2$L$^X_3$] (*X* = 1−5). The following is the procedure for the synthesis of dinuclear triple-stranded helicates for all of the ligands reported. A methanolic solution of NaOH or KOH (2 equiv with respect to the ligand) was added to a stirred suspension of the ligand in degassed methanol under an inert atmosphere. The alkaline solution was stirred until most of the solid had dissolved (approximately 10 min). $Ga(acac)_3$ (0.666 equiv) was added to the ligand, and the mixture was stirred for an additional 2−24 h at reflux. Complete evaporation of the solvent under vacuum was followed by the addition of a very small amount of degassed methanol, which dissolved most of the solids. Thoroughly degassed acetone or ether was added to the concentrated methanolic solution to precipitate the product helicate as a powder. The product was isolated via filtration under a nitrogen gas stream, washed with additional acetone, and dried in a Schlenk flask under vacuum. Alternatively, the suspended product in acetone was isolated by centrifugation followed by decanting of the supernatant and drying of the residual solid under vacuum on a Schlenk line. With either filtration or centrifugation, exposure of the product to oxygen was kept to a minimum. The dried product was transferred into an inert atmosphere box for storage and subsequent manipulations.

Acknowledgment. We thank Dr. Marco Ziegler and Professor Brice Bosnich for discussion of CD data. This work was supported by NSF Grant CHE-0317011.

Supporting Information Available: UV−vis spectrum of K$_6$[Ga$_2$**L**$^1_3$] with **s-nic**, CD spectra of **quin** and **cinc**, CD titration data for K$_6$[Ga$_2$**L**$^1_3$] with **s-nic** iodide, control VT ^{1}H NMR spectra of **s-nic** iodide and K$_6$[Ga$_2$**L**$^1_3$], ^{1}H NMR and ESI-MS data of K$_6$[Ga$_2$**L**$^5_3$]. This material is available free of charge via the Internet at http://pubs.acs.org.

IC0515711